63. *Aspidosperma* Alkaloids. A New Didehydrodimerization Mode of β-Anilinoacrylic Alkaloids by Anodic Oxidation

by **Giovanni Palmisano***, **Bruno Danieli**, **Giordano Lesma**, and **Marco Santagostino**

Dipartimento di Chimica Organica e Industriale, Università degli Studi di Milano, Centro di Studio per le Sostanze Organiche Naturali del CNR, via Venezian 21, I-20133 Milano

and **Giorgio Fiori**

Dipartimento di Chimica Fisica ed Elettrochimica, Università degli Studi di Milano, I-20133 Milano

and **Lucio Toma**

Dipartimento di Chimica Organica, Università degli Studi di Pavia, I-27100 Pavia

(31.XII.91)

A regio- and stereoselective didehydrodimerization procedure, whose key step involves the anodic oxidation, allows the conversion of β-anilinoacrylic alkaloids belonging to the *Aspidosperma* class, typified by tabersonine (**1**) and its 3-oxo derivative **2**, into the hitherto unknown 16,10′-didehydro dimers **3** and **7**, respectively.

Introduction. – In the past two and a half decades, a substantial literature has accumulated concerning the synthesis and properties of bis-indole alkaloids and their derivatives [1]. The syntheses of bis-indole alkaloids containing two different units (hetero-bis-indoles) were extensively reported, and among some of the common units which were used are *Aspidosperma* and *Corynanthé* alkaloids, vobasine, and cleavamine. One of the major challenges in this topic was the creation of the pivot bond between the 'upper' indole half (cleavamine unit) and the 'lower' indoline half (*Aspidosperma* units) in the anticancer drugs vinblastine and vincristine [2].

Our interest in the chemistry of *Aspidosperma* alkaloids prompted us to explore the dimerization of tabersonine (TBS; **1**) and of its 3-oxo analogue **2** by anodic oxidation. The strong similarity between biological and electrochemical oxidation was frequently emphasized, most recently by *Guengerich* and *MacDonald* [3]. Except for the recent isolation of voafrines by enzyme-mediated oxidation of tabersonine (**1**) [4], reports concerning the dimerization of *Aspidosperma* alkaloids are rather rare. The present investigation was undertaken to ascertain if **1** as an archetypal β-anilinoacrylic *Aspidosperma* alkaloid would undergo dimerization in an analogous manner. This is not the case, but anodic oxidation takes place to give mainly the hitherto unknown 16,10′-linked dimeric compounds, thereby disclosing a novel facet of the manifold reactivity of these important alkaloids [6] (the voltammetric behaviour of vinblastine, catharantine, and vindoline was reported [7]).

Results and Discussion. – In MeCN solutions containing 0.5M $LiClO_4$, cyclic voltammograms of tabersonine (**1**) at Pt-electrodes reflected overall irreversible oxidations, featuring a primary oxidation peak at +1.15 V (*vs.* saturated calomel electrode, SCE)

(II_a), overlapped by two other secondary peaks at 0.85 V (I_a) and +1.30 V (III_a). Preparative electrolysis of 4.5 mM **1** in MeCN at controlled potential was carried out (+1.20 V) just beyond the major oxidation peak. Electrolysis of $\geq$ 5 mM **1** resulted in formation of some dark brown, presumably polymeric, material, which was insoluble in common

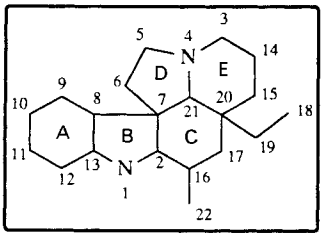

Aspidosperma biogenetic numbering

1 X = H_2
2 X = O

3 X = H_2
7 X = O

4

5

6

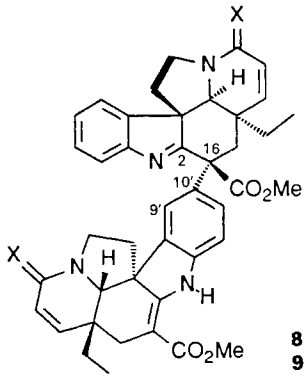

8 X = H_2
9 X = O

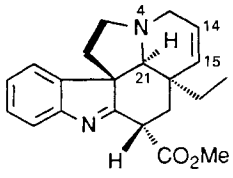

10

organic solvents. In the initial stage of electrolysis, a light blue-green colour (radical cation?) was observed near the working electrode, changing rather soon to a yellow colour which remained to the end of electrolysis.

The major product of this oxidation was the 16,10′-linked dimer **3** (46%) along with a symmetrical dimer **4** (5%), a trimer **5** (or **6**) (2%), and several other minor products which yet have to be identified. Dimer **3** was separated by column chromatography (silica gel), and dimer **4** and the unstable trimer **5** (or **6**) isolated by prep. TLC. Application of a variety of one- and two-dimensional (2D) NMR techniques established the 16,10′- and 10,10′-coupled[1]) structures for dimers **3** and **4**, respectively, whereas structure **5** (or **6**) was tentatively assigned to the trimeric compound isolated in trace amounts.

Compound **3** was obtained as a pale yellow foam (yellow colour with ceric reagent) and revealed in the EI-MS the M^+ at *m/z* 670 (20%), $C_{42}H_{44}N_4O_8$ by high resolution (HR) MS corresponding to two TBS (mol.wt. 336) units linked by a σ-bond (– 2 H). Other relevant ions were observed at *m/z* 641 (12%), 563 (11%, **a**), 419 (100%, **b**, $C_{25}H_{27}N_2O_4$ by HR-MS), and 312 (15%, **c**). Positional assignment of the two units was expected to come from collisional activation and analysis by linked-scan at constant *B/E* on the M^+ and the base peak at *m/z* 419. The fragmentation pattern $M^+ \rightarrow 641$ (– Et), 563 (– C_7H_9N), and 419 (– $C_{17}H_{19}N_2$) and *m/z* 419 → 312 (– C_7H_9N) was ascertained, thereby indicating that substitution in at least half of the molecule must be limited to ring A. The UV (MeOH) spectrum (225, 310, and 332 nm) of **3** was very similar to that of **1**, while a comparison of their IR(KBr) spectra showed that **3** had an additional strong carbonyl band at 1732 cm^{-1}.

The ^{1}H-decoupled ^{13}C-NMR ($CDCl_3$) spectrum of **3** exhibited 42 signals for the 42 C-atoms of the molecule. The DEPT spectra revealed the presence of 5 sp^3 and 10 sp^2 quaternary C-atoms, 2 sp^3 and 11 sp^2 methine C-atoms, 10 sp^2 CH_2 groups, and 4 Me groups (*Table 1*). Together they accounted for 45 protons, thereby indicating the presence of *a single* exchangeable H-atom (8.95 ppm, br. *s*) which is presumably the one attached to the indole N-atom. It could, therefore, be deduced that the two TBS units must be linked through ring A of the first unit to either N(1) or C(16) (indolenine-type substructure) of a second TBS unit. Previous chemical-shift informations on tabersonine (**1**) [9] and on the indolenine bis-indole alkaloid vincathicine [10] largely facilitated the analysis of the ^{13}C-NMR spectrum of **3**. Indeed, the chemical-shift values of the β-anilinoacrylic subunit of **3** are essentially the same as those for the corresponding C-atoms of **1**. The only C-atom which appears affected is C(10), and its lowfield shift in **3** (134.4 ppm) as compared to **1** (120.5 ppm) may be attributed to its linkage with an aryl group. The occurrence of 3 lowfield sp^2 quaternary C-atoms at 185.0 (C(2)), 152.7 (C(3)), and 147.4 (C(8)) ppm indicated that one of the TBS unit ('upper' half) should be present as an indolenine-like framework. This attribution was fully consistent with the observed chemical shifts (*i.e.*, 187.0, 154.0, and 144.2 ppm, resp.) in vincathicine. As regards the sp^3 C-atoms belonging to the 'upper' half, comparison of our ^{13}C-NMR data with those reported for **1** showed

[1]) The numbering system used throughout this work is the biogenetic numbering proposed in [8]; primed numbers refer to positions on the 'lower' unit (indoline moiety).

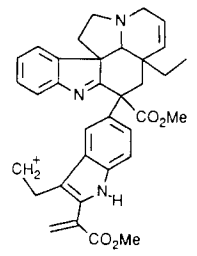

a

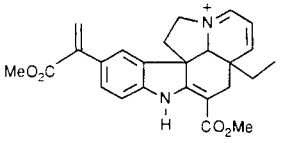

b

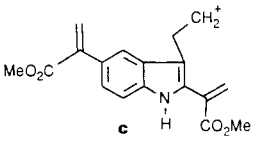

c

Table 1. *^{13}C-NMR Data* ($CDCl_3$) *of* **3** *and* **7**. δ in ppm rel. to TMS.

	C(2)	C(3)	C(5)	C(6)	C(7)	C(8)	C(9)	C(10)	C(11)	C(12)	C(13)	C(14)	C(15)	C(16)	C(17)
3	185.0	50.4	50.9	36.9	61.7	147.4	121.2	127.5	126.1	120.9	152.7	125.0	134.2	55.0	41.9
7	180.1	161.1	44.4	36.1	56.7	145.0	122.3	128.8	127.6	120.7	153.1	124.1	146.6	63.2	39.0

	C(18)	C(19)	C(20)	C(21)	C(22)	C(23)	C(2′)	C(3′)	C(5′)	C(6′)	C(7′)	C(8′)	C(9′)	C(10′)
3	8.4	27.2	41.2	71.8	173.9	52.7	166.8	50.4	52.9	44.4	56.0	137.8	120.9	134.4
7	9.5	27.5	40.5	66.5	172.4	53.4	165.0	161.6	43.6	43.5	54.7	136.3	120.2	133.8

	C(11′)	C(12′)	C(13′)	C(14′)	C(15′)	C(16′)	C(17′)	C(18′)	C(19′)	C(20′)	C(21′)	C(22′)	C(23′)
3	127.0	108.8	142.2	125.5	133.0	92.5	29.0	7.4	26.7	41.2	69.4	168.8	50.9
7	127.2	109.6	142.7	123.1	145.3	91.2	26.2	7.5	27.1	39.9	65.6	168.3	51.4

nearly identical values, except for the resonances of C(16), C(17), and C(6) which are now displaced to 55.0 (*vs.* 92.5 in **1**), 41.9 (*vs.* 26.7), and 36.9 (*vs.* 44.3) ppm, respectively, mirroring the structural alteration in dimer **3**.

The structural assignment of **3** was confirmed by use of conventional and 2D-NMR techniques, including ^{1}H,^{1}H COSY, ^{1}H,^{13}C heteronuclear COSY through direct and long-range couplings. In particular, the presence of 2 *d* (each 1H) for 2 vicinal protons in the lowfield aromatic region at 7.13 and 6.71 ppm (J = 7.9 Hz), which were assigned to H–C(11′) and H–C(12′), respectively, implies that C(10′) must be involved in the bond connecting the two TBS units (*Table 2*). Accordingly, the remaining aromatic proton of the 'lower' subunit at 7.15 ppm (1H) appeared as a br. *s* and was assigned to H–C(9′). The strong NOE between the indole NH and H–C(12′) due to their close spatial relationship (*peri* interaction) is also in accordance with these assignments.

Table 2. *^{1}H-NMR Data* (300 MHz, $CDCl_3$) *of* **3**, **4**, *and* **7**. δ in ppm rel. to TMS, J in Hz.

	3	**7**	**4**
H_α–C(3)	3.06 (br. *d*, J = 16.0)	–	3.22 (br. *d*, J = 16.0)
H_β–C(3)	3.40 (br. *dd*, J = 16.0, 4.2)	–	3.48 (br. *dd*, J = 16.0, 5.0)
H_α–C(5)	2.69 (*dt*, J = 11.8, 4.2)	3.46 (*ddd*, J = 12.0, 12.0, 4.8)	2.75 (*m*)
H_β–C(5)	*ca.* 3.0 (*m*)	4.11 (*dd*, J = 12.0, 7.8)	3.07 (*ddd*, J = 7.0, 6.0, 1.5)
H_α–C(6)	1.50 (*dd*, J = 11.8, 4.2)	1.52 (*dd*, J = 12.0, 4.8)	1.88 (*dd*, J = 11.0, 5.0)
H_β–C(6)	2.07 (*dt*, J = 11.8, 11.8, 6.8)	1.90 (*ddd*, J = 12.0, 12.0, 7.8)	2.11 (*dt*, J = 11.0, 11.0, 7.0)
H–C(9)	7.69 (*d*, J = 7.7)	7.79 (br. *d*, J = 7.5)	7.35 (*d*, J = 7.5)
H–C(10)	7.35 (*t*, J = 7.7)	7.42 (br. *d*, J = 7.5)	–
H–C(11)	7.21 (*t*, J = 7.7)	7.28 (br. *t*, J = 7.5)	7.33 (*t*, J = 7.5)
H–C(12)	7.35 (*d*, J = 7.7)	7.36 (br. *d*, J = 7.5)	6.85 (*d*, J = 7.5)
H–C(14)	5.72 (br. *dd*, J = 10.0, 4.2)	5.97 (*d*, J = 10.0)	5.80 (br. *dd*, J = 9.5, 5.0)

Table 2 (cont.)

	3	**7**	**4**
H–C(15)	5.60 (br. *d*, *J* = 10.0)	6.28 (*d*, *J* = 10.0)	5.71 (br. *d*, *J* = 9.5)
H_α–C(17)	2.91 (br. *d*, *J* = 14.2)	3.10 (*dd*, *J* = 14.0, 2.1)	2.56 (br. *d*, *J* = 15.0)
H_β–C(17)	3.18 (*d*, *J* = 14.2)	2.53 (*d*, *J* = 14.0)	2.45 (*d*, *J* = 15.0)
H–C(18)	0.47 (*t*, *J* = 7.2)	0.58 (*t*, *J* = 7.2)	0.66 (*t*, *J* = 7.5)
$H_{pro\text{-}R}$–C(19)	0.92 (*dd*, *J* = 14.0, 7.2)	0.93 (*dq*, *J* = 14.0, 7.2)	0.80 (*q*, *J* = 7.5)
$H_{pro\text{-}S}$–C(19)	1.30 (*dd*, *J* = 14.0, 7.2)	1.59 (*dq*, *J* = 14.0, 7.2)	1.05 (*d*, *J* = 7.5)
H–C(21)	2.80 (br. *s*)	4.17 (*d*, *J* = 2.0)	2.73 (br. *s*)
MeO	3.70 (*s*), 3.72 (*s*)	3.70 (*s*), 3.75 (*s*)	3.78 (*s*)
H_α–C(3′)	*ca.* 3.0 (*m*)	–	
H_β–C(3′)	3.39 (br. *dd*, *J* = 16.0, 4.0)	–	
H_α–C(5′)	2.68 (*ddd*, *J* = 11.8, 8.6, 4.4)	3.36 (*dt*, *J* = 11.7, 9.0, 9.0)	
H_β–C(5′)	*ca.* 3.0 (*m*)	4.29 (*ddd*, *J* = 11.7, 5.8, 2.1)	
H_α–C(6′)	1.82 (*dd*, *J* = 11.8, 4.4)	*ca.* 1.92 (*m*)	
H_β–C(6′)	2.03 (*dt*, *J* = 11.8, 6.0)	*ca.* 1.92 (*m*)	
H–C(9′)	7.15 (br. *s*)	7.18 (*d*, *J* = 1.6)	
H–C(10′)	–	–	
H–C(11′)	7.13 (br. *d*, *J* = 7.9)	7.17 (*dd*, *J* = 8.3, 1.6)	
H–C(12′)	6.71 (*d*, *J* = 7.9)	6.76 (*d*, *J* = 8.2)	
H–C(14′)	5.73 (br. *dd*, *J* = 10.0, 4.0)	5.92 (*d*, *J* = 10.0)	
H–C(15′)	5.49 (br. *d*, *J* = 10.0)	6.38 (*d*, *J* = 10.0)	
H_α–C(17′)	2.48 (*d*, *J* = 15.0)	2.57 (*dd*, *J* = 15.2, 1.9)	
H_β–C(17′)	2.41 (*d*, *J* = 15.0)	2.03 (*d*, *J* = 15.2)	
H–C(18′)	0.53 (*t*, *J* = 7.2)	0.65 (*t*, *J* = 7.2)	
$H_{pro\text{-}R}$–C(19′)	0.76 (*dd*, *J* = 14.0, 7.2)	0.99 (*dq*, *J* = 14.0, 7.2)	
$H_{pro\text{-}S}$–C(19′)	0.95 (*dd*, *J* = 14.0, 7.2)	1.04 (*dq*, *J* = 14.0, 7.2)	
H–C(21′)	2.49 (br. *s*)	3.79 (*d*, *J* = 1.9)	
NH	8.95 (br. *s*)	9.03 (br. *s*)	

Extensive ^{1}H-difference NOE studies were carried out next to define the configuration at the newly formed asymmetric center C(16). The fact that the H_β–C(16) and both H–C(17) resonances were enhanced upon saturation of the H–C(9′)/H–C(11′) resonances (*vide infra*) in addition to the observed downfield shift for C(6) support the proposed configuration at C(16) of **3**. No NOE between these protons would be expected for the (16*S*)-diastereoisomer **8** (*vide infra*).

To rationalize the configurational outcome of the substitution event, we assume that the developing 1,3-diaxial interaction between the incoming electrophile (TBS unit) and the Et chain at C(20) retards attack on the α-face. β-Face attack thus lead to the emergence of the dimer **3** with the 'lower' half at C(16) equatorially β-oriented. It should be pointed out that the high degree of face selectivity is in agreement with what is generally found for an electrophilic attack on β-anilinoacrylic *Aspidosperma* alkaloids [11].

Furthermore, we attempted to settle the gross conformation of **3** by rotation around the pivot bond using interunit NOE's. In particular, the interunit NOE's between H–C(9′), H–C(11′), and CH_2(17) are important because they should reveal the spatial relationship between both units and thus the overall conformation of **3**. Disappointingly, the chemical shifts of H–C(9′) and H–C(11′) are too close (7.15 and 7.13 ppm, resp.) to unambiguously assign the observed NOE's to *H*–C(9′),C*H*$_2$(17) rather than to *H*–C(11′),C*H*$_2$(17).

The EI-MS of **4** (blue spot with ceric reagent) showed M^+ at *m/z* 670 indicating the molecular formula $C_{42}H_{46}N_4O_4$ which could be confirmed by HR-MS. The 300-MHz ^{1}H-NMR ($CDCl_3$) of **4** (*Table 2*), as compared with that of **1**, showed changes in the lower-field region (the *t* for H–C(10) of **1** was missing), while the upfield region strictly resembled that of **1**. Accordingly, H–C(9) and H–C(11) appeared as *s* (7.35 ppm) and *d* (7.33 ppm), respectively, both deshielded and broad, instead of a *d* and *t* in **1**. These observations can be explained by assuming the presence of an aryl group at C(10), leading to the observed downfield shifts for H–C(9) (0.14 ppm) and H–C(11) (0.21 ppm). The structure of dimer **4** thus has C_2 symmetry with a twofold axis lying perpendicular to the plane containing rings A and A′ and intersecting the pivot bond.

The EI-MS of the short lived trimer (yellow spot with ceric reagent) failed to give significant peaks above 650 m.u. Using the fast atom bombardment (FAB) technique, however, an intense quasi-molecular ion was observed at *m/z* 1005 (MH^+) corresponding to a molecular formula ($M^{+\cdot}$) $C_{63}H_{68}N_6O_6$ (*i.e.*, 3 TBS – 6 H). The ^{1}H-NMR spectrum showed 3, aliphatic *t* at 0.27, 0.42, and 0.50 ppm due to CH_3(18), 3 sets of *d*'s at 1.50, 1.56, and 1.76 (H_z–C(6)) strongly coupled with 3 *dt* (1.97, 1.99, and 2.12 ppm) assigned to H_β–C(6). Moreover, 3 sharp *s* (3.16 (2 × *s*) and 3.66 ppm) for COOMe as well as 3 *d* at 5.33, 5.43, and 5.55 ppm for H–C(15) were also present. But apart form the presence of 1 NH signal (8.85 ppm) and 3 *d* (each 1H) for vicinal aromatic protons (6.62, 7.49, and 7.61 ppm), severe crowding in the region 6.5–8.0 ppm precluded an exhaustive assignment of aromatic protons. Thus, evidence to distinguish between the more plausible isomer **5** and **6** was not unambiguously available from the above data, and further spectral studies were hampered by the paucity and the instability of this material.

Convinced that anodic oxidation of β-anilinoacrylic *Aspidosperma* alkaloids represents an efficient and unique approach to novel didehydro dimers, we next investigated the electrochemical behaviour of 3-oxotabersonine (**2**), an alkaloid isolated from the seeds of *Amsonia elliptica* and easily available by $KMnO_4$ oxidation of tabersonine (**1**) [12]. Thus, when 5.0 mM **2** in MeCN containing 0.5M $LiClO_4$ was subjected to the controlled-potential electrolysis (1.20 V(SCE))[2], a quite clean transformation (TLC) was observed and the didehydro dimer **7** (68%) accompanied only by starting **2** was obtained.

HR-MS of **7** gave a molecular formula $C_{42}H_{42}N_4O_6$ (dimer **3**, $C_{42}H_{46}N_4O_4$). Collision activation and analysis by linked scan at constant *B/E* showed the following characteristic fragmentation pattern: *m/z* 698→575 (–123), 265 (–433), and 433 (–265), and *m/z* 575→452 (–123), 265 (–310). The major feature were a loss of 123 m.u. (**d**) from $M^{+\cdot}$ to give ion **e** (*m/z* 575) and the presence of ion **f** (*m/z* 433). The ^{13}C-NMR spectrum (*Table 1*) of **7**, assigned by heteronuclear correlation experiments, showed that the main differences between **3** and **7** are associated with the presence of the keto function at C(3). Furthermore, the ^{1}H-NMR of **7** (*Table 2*), with the exception of few signals, is strikingly similar to that of **3**. Likewise in **3**, the H–C(9′) signal is too close to H–C(11′) to allow a meaningful NOEDS experiment in order to ascertain the overall conformation(s). However, as in dimer **3**, the attachment of the monomeric units is at C(16) and C(10′) with the substituent at C(16) likely to be on the β-face due to steric factors.

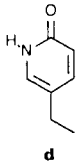

d

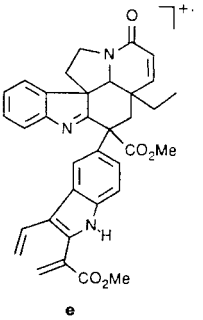

e

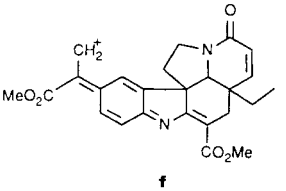

f

[2]) Cyclic voltammetry of **2** gave no evidence for reversibility of any of the voltammetric peaks (+1.07, +1.26 V *vs.* SCE).

To gain some further insight in the structural features of dimers **3** and **7**, we undertook empirical force-field (EFF) calculations. First, we employed *Allinger*'s MM2(85) [13] program for energy minimization of the two possible 16-diastereoisomers **3** and **8** that possibly arise on dimerization of tabersonine (**1**). The model compounds **1** and its 16*H*-tautomer **10** were used for a calculation approach to elucidate the role of the configuration at C(16) in the dimeric compounds **3** and **8**. The model compounds have a rigid pentacyclic moiety, while the conformational flexibility due to D/E rings leads to a multiplicity of possible conformations. Accordingly, N(4) inversion interchanges the relative *cis-trans*-arrangement of H–C(21) and the lone pair at N(4). The calculations showed that the *trans*-fusion (rings C/D) is preferred for **1** (*ca.* 1 kcal/mol) and for **10** (*ca.* 2 kcal/mol). As this arrangement deeply influences the conformation of ring E, the vicinal coupling constants for CH_2(5) and CH_2(6) were calculated [14] from the optimized *cis*- and *trans*-geometries of **1** and **10**, and then compared with the experimental values found for **3**. The close agreement between the experimental data and the values calculated for the optimized geometries *trans*-**1** and *trans*-**10** (C/D *trans*-fusion) allowed to conclude that the *trans*-isomer is largely preferred in both monomeric models. Any attempts to verify the reliability of the EFF analysis of **1** by single-crystal X-ray crystallography were precluded by the twinning of the thin crystal of **1** obtained. However, the structure of the closely related vincadifformine (=14,15-dihydro-TBS) was unambiguously established by X-ray analysis, fundamentally matching the structural parameters calculated for the ground-state conformation *trans*-**1** of TBS [15]. Accordingly, in the ensuing analysis of the dimeric structures **3** and **8**, the *cis*-arrangement was not considered further. The preferred orientation of the Et group at C(20) as well of the COOMe group at C(16) in **1** and **10** was not taken into account as their orientation would be optimized again in **3** and **8**.

The EFF investigations of dimer **3** was mainly focused on the determination of the freedom of rotation around the pivot bond C(16)–C(10′). Full-range scan of torsional angle C(2)–C(16)–C(10′)–C(9′) allowed the determination of two minima. For both geometries, the conformational space relative to the rotation of the Et and COOMe group linking them to the dimeric framework was explored. The data reported in *Table 3* and the plots depicted in *Fig. 1* for the conformers **3A** ('open conformation'; 0.0 kcal/mol)

Table 3. *Relative Steric Energies and Selected Geometrical Features of Compounds* **3**, **8**, **7**, *and* **9**

	3A	**3B**	**8A**	**8B**	**7A**	**7B**	**9A**	**9B**
E_{rel} [kcal/mol]	0.0	1.2	2.3	3.9	0.0	1.5	2.6	4.1
Torsional angles [°]								
C(2)–C(16)–C(10′)–C(9′)	22	–163	28	–157	19	–164	15	–168
C(2)–C(16)–C(22)–O	–82	–82	59	61	–79	–79	61	63
C(18)–C(19)–C(20)–C(21)	60	60	72	69	61	61	–177	–178
C(2′)–C(16′)–C(22′)–O	–7	–7	–6	–6	–6	–6	–5	–6
C(18′)–C(19′)–C(20′)–C(21′)	65	63	64	64	64	64	64	64
H–H distances [Å]								
H_α–C(17),*H*–C(9′)	4.92	2.44	3.69	2.93	4.88	2.36	4.07	2.52
H_β–C(17),*H*–C(9′)	4.23	2.46	4.58	3.46	4.13	2.59	4.72	3.49
H_α–C(17),*H*–C(11′)	2.49	4.92	2.89	3.70	2.42	4.89	2.63	4.17
H_β–C(17),*H*–C(11′)	2.49	4.21	3.51	4.62	2.64	4.15	3.56	4.78

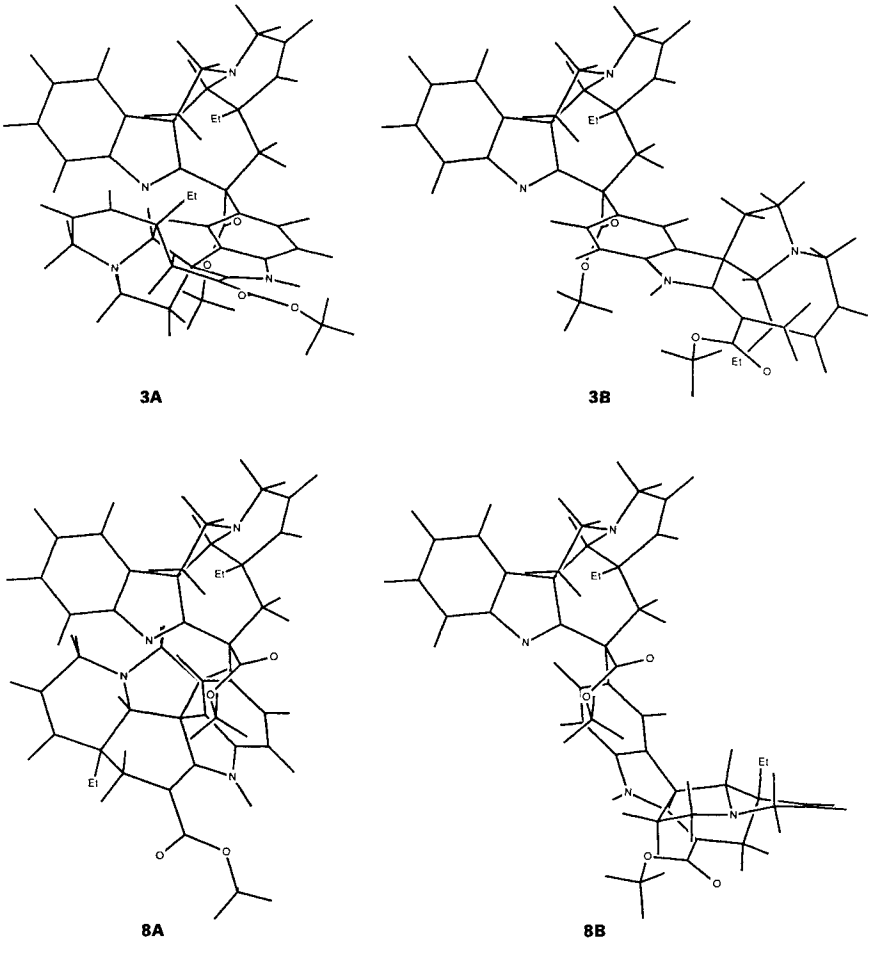

Fig. 1. *MM2-Optimized geometries of compounds* **3** *and* **8**

and **3B** ('closed conformation'; 1.2 kcal/mol) refer to the lowest of the minima obtained from these rotations. In *Table 3* are also reported the distances between H–C(9′) (and H–C(11′)) and the diastereoisotopic CH_2(17) protons. When the same strategy was followed for (16*S*)-diastereoisomer **8**, two different minima for rotation around bond C(16)–C(10′) were located. The low-energy structures **8A** (2.3 kcal/mol) and **8B** (3.9 kcal/mol) exist with the CH_2(17) protons canted away from H–C(9′) and H–C(11′), and as can be seen in *Table 3*, the network of interunit short distances (< 3 Å) in both conformers is much less extended.

In an attempt to gain more insight concerning the conformational feature of the dimerization product of **2**, detailed EFF calculations were performed on **7** and its (16*S*)-diastereoisomer **9**. They led to the same conclusion as for the dimers **3** and **8**, respectively; the results are summarized in *Table 3* and *Fig. 2*.

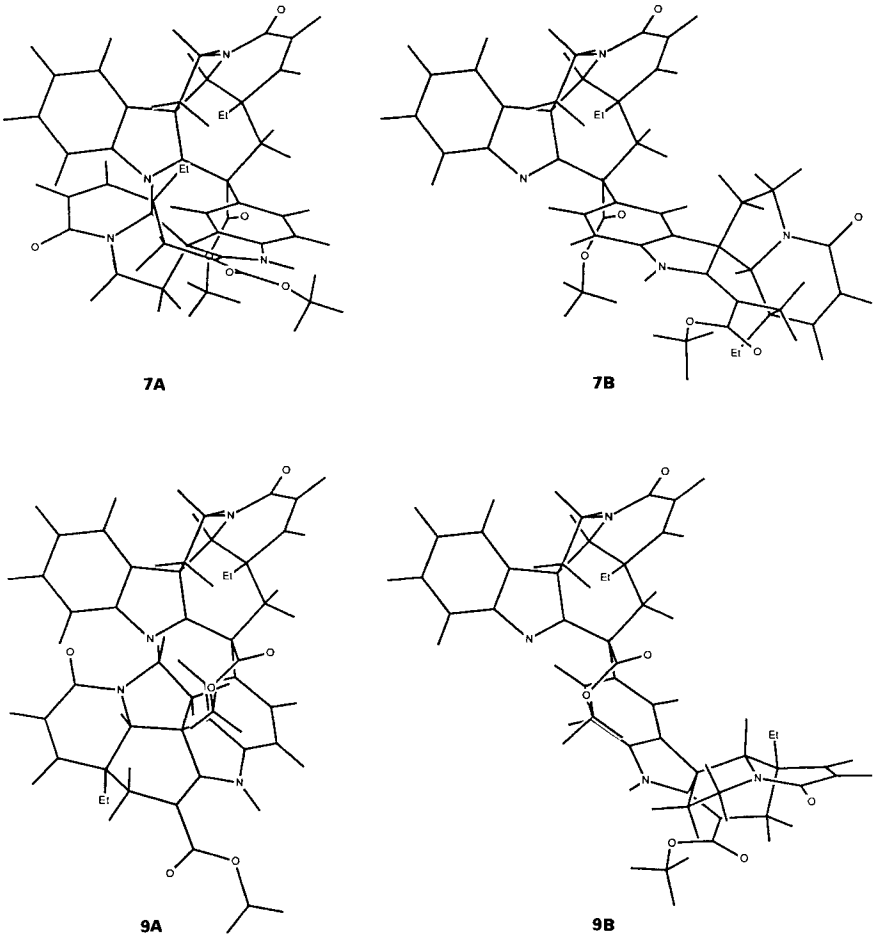

Fig. 2. *MM2-Optimized geometries of compounds* **7** *and* **9**

Three main pathways can be considered for the mechanism of the electrochemical didehydrodimerization processes. Two involve initial one-electron abstraction followed either by coupling of the resultant radicals (radical-radical coupling) or attack by the radical on the parent compound (radical-substrate coupling). The third possibility involves a two-electron abstraction to yield a divalent compound (ion-substrate coupling) [16]. The very distorted shape of the voltammetric peaks for **1** and **2** at the Pt anode and the totally irreversible nature of the electrode processes precluded any meaningful investigation of the electrode mechanism by use of cyclic voltammetry or chronoamperometric or potentiostatic experiments. Irreversibility implies that the species formed upon oxidation undergoes some other process faster than it can be reduced back to the oxidation precursor. The typical processes that might interfere with reduction include a subsequent chemical reaction, a conformational change, or absorption of the oxidized species onto the

electrode surface [17]. Nevertheless, considering the product formed in the peak at 1.15 V for **1** give some clues on the electrode reactions and mechanism. Accordingly, we propose that electrochemical oxidation of tabersonine **1** proceeds by the initial one-electron abstraction to form radical cation $\mathbf{1}^{+\cdot}$. It is reasonable to assume that in $\mathbf{1}^{+\cdot}$ the electron is removed from N(1), the SOMO (singly occupied molecular orbital) resulting from mixing of the p-type lone-pair N-orbital and the symmetrical π MO of the aromatic ring. Deprotonation of $\mathbf{1}^{+\cdot}$ would then give a neutral radical $\mathbf{1}^{\cdot}$ which is further oxidized to the

Scheme

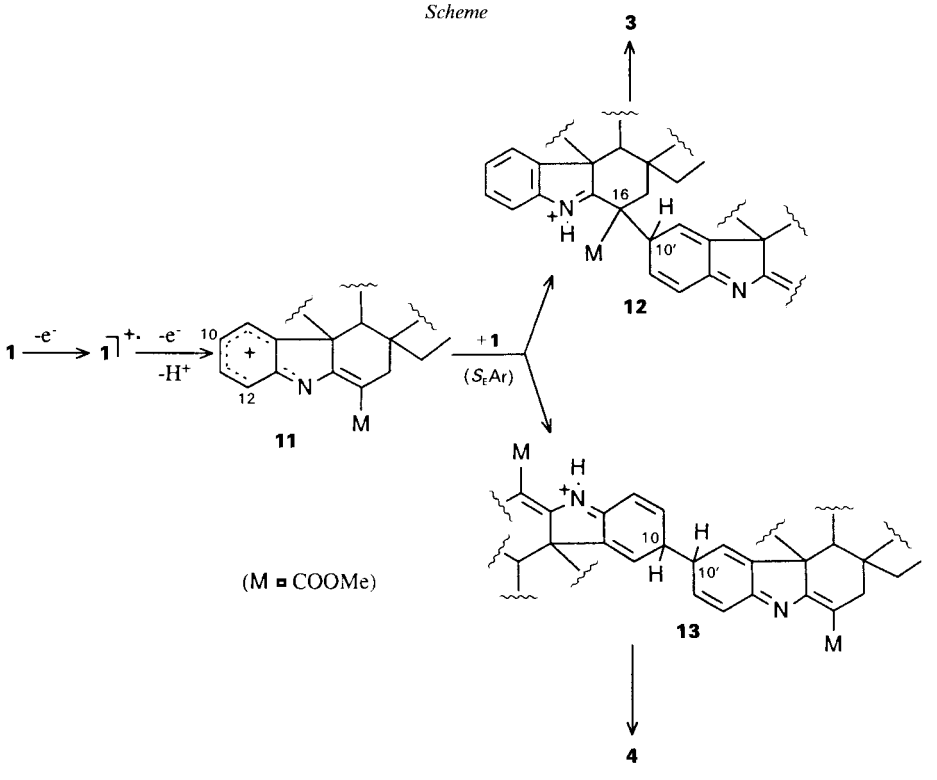

nitrenium ion **11** (*Scheme*). A plausible route then involves nucleophilic attack of **1** in a sequence that leads to dimeric (or polymeric) compounds. The dimer formed in highest yield is 16*β*-(tabersonin-10′-yl)-tabersonine (**3**), and all other isolated compounds have at least one TBS residue linked to the C(10) position. This suggests that the predominant form of the radical cation $\mathbf{1}^{+\cdot}$ generated in the initial electron transfer from **1** has the unpaired electron essentially located at C(10). Furthermore, it was shown that the positive-charge density in the *para* position (*i.e.* at C(10)) of the singlet-state nitrenium ions is much larger than that in the *ortho* position (*i.e.*, C(12)) [18]. The fact that dimer **4** (linked at the 10,10′-positions) was isolated is in line with the well documented proclivity of *β*-anilinoacrylic *Aspidosperma* alkaloids to undergo electrophilic attack at C(16) and/or C(10) positions [19]. On the other hand, it is intuitive that attack at C(16) *vs.* C(10)

should increase the stability of the intermediate *Wheland* σ-complex **12** *vs.* **13**, thereby favouring coupling of C(16) of **1** with **11**.

The chemistry at the electrode surface becomes extremely complex as a result of secondary reactions between **11** and the dimer **3** and **4** to yield **5** (or **6**). It is likely that many other similar oligomerization reactions occur, and the polymeric material formed as a result of exhaustive electrooxidation of more concentrated solutions of **1** no doubt represents the ultimate product of these types of reactions.

Finally, this paper discloses the ability of β-anilinoacrylic alkaloids belonging to the *Aspidosperma* class, typified by tabersonine (**1**) and 3-oxotabersonine (**2**), to undergo a novel didehydrodimerization mode and, meanwhile, highlights the potential of electrochemical approaches for the synthesis of compounds not available by any conventional procedure.

Experimental Part

General. Compounds were detected on developed chromatograms by fluorescence quenching (254 or 365 nm) or visualized with cerium(IV) ammonium sulfate (1% in 85% H_3PO_4). IR Spectra: *Perkin-Elmer-681* spectrophotometer. UV Spectra: *Perkin-Elmer-554* UV/VIS spectrophotometer. NMR Spectra: *Bruker CPX-300* instrument; chemical shifts δ in ppm downfield from TMS, coupling constants J in Hz. EI-MS (70 eV), HR-MS ($R = 5000$), and FAB-MS (pos. mode, glycerol matrix): *VG-70-70-EQ* instrument.

Anodic Oxidation of Tabersonine (**1**). In the anode chamber of a three-compartment cell (H-type) with Pt electrode (10 cm^2) and saturated calomel electrode (SCE) is introduced **1** (61 mg, 0.18 mmol) in 0.5M $LiClO_4$ in MeCN (40 ml). In the cathode compartment is introduced 0.5M $LiClO_4$ in MeCN (40 ml). The soln. is magnetically stirred at r.t. under N_2 and electrolyzed at +1.20 V (SCE). In the initial stage of electrolysis, a green-blue colour was observed near the working electrode, changing rather soon to a yellow colour which remained to the end of electrolysis. The electrolysis was terminated when the current reached a steady, low value, corresponding to the transfer of 2.1 F/mol. After evaporation at r.t., the resulting brown residue was suspended in 5% $NaHCO_3$ soln. and extracted with AcOEt (3 × 50 ml). The combined org. phases were dried ($MgSO_4$) and evaporated to leave a brown residue (84 mg). Column chromatography (silica gel, CH_2Cl_2) gave the major product **3** (R_f (CH_2Cl_2/Et_2O/Et_3N 15:5:0.1) 0.56; 56 mg) and a mixture of minor compounds with unreacted **1**. This mixture was subjected to prep. TLC (silica gel, Et_2O/Et_2NH 10:0.1). The bands were visualized with UV light, removed, and eluted with AcOEt. The major band (2nd from top) gave pure **4** (R_f 0.50; 6 mg); crude **5** (or **6**) (6th from top) and **1** (3 mg) were also recovered. The crude **5** (or **6**; 5 mg) was further purified by MPLC (Et_2O/Et_2NH 10:0.1) to yield pure **5** (or **6**) (R_f 0.26; 2 mg).

Data of (16R)-16-(Tabersonin-10′-yl)tabersonine (**3**). Pale yellow foam. UV (MeOH): 225, 310 (sh), 332. IR ($CHCl_3$): 3380, 1727, 1660, 1600. EI-MS: 698 (8), 640 (9), 575 (41), 395 (8), 375 (10), 361 (22), 277 (17), 265 (45), 250 (24), 237 (17), 167 (19).

Data of 10-(Tabersonin-10′-yl)tabersonine (**4**). Pale yellow glass. IR ($CHCl_3$): 3430, 3370, 1670, 1610, 1480. EI-MS: 670 (5), 552 (9), 537 (8), 523 (10), 368 (13), 336 (10), 313 (12), 236 (15), 214 (23), 167 (58).

Anodic Oxidation of 3-Oxotabersonine (**2**). The same procedure as for **1** starting with **2** (70 mg) at 1.20 V (SCE) (1.5 F/mol transfer) gave, after prep. TLC (Et_2O/Et_2NH, 10:1), pure **7** (89 mg).

Data of (16R)-3-Oxo-16-(3′-oxotabersonin-10′-yl)tabersonine (**7**). Colourless foam. UV (MeOH): 265, 290, 332. IR ($CHCl_3$): 3380, 1727, 1660, 1600. EI-MS: 698 (8), 640 (9), 575 (41), 395 (8), 375 (10), 361 (22), 277 (17), 265 (45), 250 (24), 237 (17), 167 (19).

We gratefully acknowledge financial support provided by the *Ministero della Università e della Ricerca Scientifica e Tecnologia* (*MURST*, Piano 40%). We also express our thanks to Mr. *B. Vodopivec* for preliminary electrochemical experiments.

REFERENCES

[1] M. Lounasmaa, A. Nemes, *Tetrahedron* **1982,** *38,* 223; G. Cordell, 'The Bisindole Alkaloids' in 'Indoles. Part IV', Ed. J.E. Saxton, John Wiley, New York, 1983, pp. 467–728.

[2] For recent advances, see: M.E. Kuehne, I. Markò, 'Synthesis of Vinblastine-type Alkaloids', in 'The Alkaloids', Ed. A. Brossi, Academic Press, San Diego, 1990, Vol. 37, pp. 77–131.

[3] F.P. Guengerich, T.L. MacDonald, *Acc. Chem. Res.* **1984,** *17,* 9. For recent results, see M.Z. Wrona, G. Dryhurst, *Bioorg. Chem.* **1990,** *18,* 291.

[4] a) J. Stöckigt, K.-H. Pawelka, T. Tanahashi, B. Danieli, W.E. Hull, *Helv. Chim. Acta* **1983,** *66,* 2525; b) H. Schübel, W. Fahn, J. Stöckigt, *ibid.* **1989,** *72,* 147.

[5] a) H.J. Rosenkranz, B. Winkler-Lardelli, H.J. Hansen, H. Schmid, *Helv. Chim. Acta* **1974,** *57,* 877; b) Erra-Balsells, *Phytochemistry* **1988,** *27,* 3945; c) F.S. Saralsani, M.W. Duffel, J.P. Rosazza, *J. Med. Chem.* **1985,** *28,* 629; d) H. Bölcskei, E. Gàcs-Baitz, Cs. Szàntay, *Tetrahedron Lett.* **1989.** *28,* 7245.

[6] G. Palmisano, B. Danieli, G. Lesma, T. Pilati, F. Trupiano, *J. Org. Chem.* **1988,** *53,* 1056, and ref. cit. therein.

[7] J.F. Rusling, B.J. Scheer, I.U. Haque, *Anal. Chim. Acta* **1984,** *158,* 23; see also G.T. Cheek, R.F. Nelson, J.M. Bobbitt, P.M. Scola, *J. Org. Chem.* **1987,** *52,* 5277; S. Longchamp, G. Barbey, P. Granger, *New J. Chem.* **1989,** *13,* 525.

[8] J. Le Men, W.I. Taylor, *Experientia* **1965,** *21,* 508.

[9] E. Wenkert, D.W. Cochran, E.E. Hagaman, F.M. Schell, N. Neuss, A.S. Katner, P. Potier, C. Kan, M. Plat, M. Koch, H. Mehri, T. Poisson, N. Kunesch, Y. Rolland, *J. Am. Chem. Soc.* **1973,** *95,* 4990.

[10] S.S. Tafur, J.L. Occolowitz, T.K. Elzey, J.W. Paschal, D.E. Dorman, *J. Org. Chem.* **1976,** *41,* 1001.

[11] a) J. Lévy, C. Pierron, G. Lukacs, G. Massiot, J. Le Men, *Tetrahedron Lett.* **1976,** 669; b) G. Hugel, J. Lévy, *Tetrahedron* **1983,** *39,* 1539; c) B. Danieli, G. Lesma, G. Palmisano, R. Riva, *J. Chem. Soc., Chem. Commun.* **1984,** 909.

[12] N. Aimi, Y. Asada, S.-I. Sakai, J. Haginiwa, *Chem. Pharm. Bull.* **1978,** *26,* 1182.

[13] J.C. Tai, N.L. Allinger, *J. Am. Chem. Soc.* **1988,** *110,* 2050.

[14] C.A.G. Haasnoot, F.A.A.M. de Leeuw, C. Altona, *Tetrahedron* **1980,** *36,* 2783.

[15] G. Palmisano, T. Pilati, submitted to *Acta Crystallogr., Sect. A.*

[16] a) C.P. Andrieux, L. Nadjo, J.M. Savéant, *J. Electroanal. Chem. Interfacial Electrochem.* **1970,** *26,* 147; b) L. Nadjo, J.M. Savéant, *ibid.* **1973,** *44,* 327.

[17] See *e.g.:* R.P. Thummel, I. Lefoulon, S. Chirayil, V. Goulle, *J. Org. Chem.* **1988,** *53,* 4745.

[18] Y. Li, R.A. Abramovitch, K.N. Houk, *J. Org. Chem.* **1988,** *54,* 2911.

[19] See *e.g.:* G. Lewin; Y. Rolland, J. Poisson, *Heterocycles* **1990,** *14,* 1916.